ADVANCED OPTICAL MATERIALS
www.advopticalmat.de

Cellulose-Assisted Formation of 2D Hybrid Halide Perovskite Nanocrystals with Enhanced Stability for Light-Emitting Devices

Susana Ramos-Terrón, Lea Spitzer, Cristina Martín, Eduardo Solano, Daniel Hermida-Merino, Sébastien Lecommandoux, François Jérôme, Henri Cramail, Pablo G. Argudo, and Gustavo de Miguel**

A common approach to enhance the stability of metal halide perovskites (MHPs) implemented in optical and optoelectronic devices is to incorporate polymer additives into the perovskite layer. A β-(1,4) cellulose oligosaccharide (COS) synthesized by mechanocatalytic depolymerization of cellulose has been incorporated to films of the $BA_2MA_4Pb_5I_{16}$ (BA = *n*-butylammonium and MA = methylammonium) two-dimensional (2D) Ruddlesden-Popper (RP) hybrid perovskite. Scanning Electron Microscopy (SEM) images displayed a three-fold reduction of the 2D RP perovskite grains (≈30–40 nm), close to the quantum confinement scale. The analysis of the dark *J–V* curves of single carrier devices by using the space charge limited current (SCLC) method resulted in a rise of the defect concentration. A notable 14-fold increase in the photoluminescence (PL) signal at high COS content is detected. Moreover, the analysis of the temperature dependence PL measurements (80–300 K) resulted in a larger exciton binding energy, Eb = 180 to 370 meV, at high COS content. Light emitting diodes of the 2D RP perovskites (PeLEDs) are fabricated w/o the COS compound. The stability test performed under operation (5 V) displays 20 times higher operational lifetimes at high COS content while the luminance is also increased in the devices with the COS compound.

1. Introduction

Metal halide perovskites (MHPs) have already established themselves as the most promising material for emerging photovoltaic devices.[1–4] The outstanding optoelectronic properties of the MHPs make them excellent candidates for many other applications such as light-emitting diodes,[5,6] X-ray photodetectors,[7,8] field-effect transistors[9,10] or lasers.[11,12] In particular, the use of MHPs nanocrystals (NCs), quasi-2D MHPs, and, more recently, the use of core/shell MHPs NCs[13–20] in perovskite light-emitting diodes (PeLEDs) has experienced a remarkable development, at a level similar to that of the perovskite solar cells.[21] Even though PeLEDs devices offer several advantages, as a high external quantum efficiency (EQE), ease of tuning the emission wavelength, narrow linewidth of the emission, and intrinsic high photoluminescence quantum yields (PLQYs),[6,22–24] there are still some limitations like the brightness, operational

S. Ramos-Terrón, G. de Miguel
Departamento de Química Física y Termodinámica Aplicada
Instituto Químico para la Energía y el Medioambiente (IQUEMA)
Universidad de Córdoba
Campus de Rabanales
Edificio Marie Curie
Córdoba E-14071, Spain
E-mail: gmiguel@uco.es

L. Spitzer, S. Lecommandoux, H. Cramail, P. G. Argudo
Université de Bordeaux
CNRS
Bordeaux INP
LCPO
UMR 5629
Pessac F-33600, France
E-mail: argudop@mpip-mainz.mpg.de

L. Spitzer, F. Jérôme
Institut de Chimie des Milieux et Matériaux de Poitiers
CNRS
Université de Poitiers
1 rue Marcel Doré, cedex 9, Poitiers 86073, France

C. Martín
Department of Physical Chemistry
Faculty of Pharmacy
University of Castilla-La Mancha
Albacete 02071, Spain

The ORCID identification number(s) for the author(s) of this article can be found under https://doi.org/10.1002/adom.202300676

DOI: 10.1002/adom.202300676

lifetime and the long-term instability of MHPs under harsh environments, e.g., heat,[25,26] light[27] and moisture.[28]

A common approach to overcome the existing drawbacks of PeLEDs is to incorporate different types of polymer additives into the MHPs films[29,30] which is a strategy borrowed from the technology of perovskite solar cells (PSCs).[13,28,31–34] The addition of the polymer chains is typically achieved by blending them with colloidal MHPs nanocrystals or with the MHPs precursors to fabricate thin films.[13,35] For instance, the incorporation of poly(maleic anhydride-alt-1-octadecene) (PMA) polymer during the synthesis of β-$CsPbI_3$ nanocrystals[36] can regulate their crystallization kinetics and reduce deep defects by forming Pb–O bonds that passivate the NCs surface. The addition of the PMA polymer results in improved device performance, including a three-fold increase in PLQY, superior operational stability (T_{50} = 317 hours), and a higher EQE (17.8%).[36]

However, the impact of the polymer depends on its ratio to the MHPs precursors. Low levels of the polymer (1–5 wt.% or 0.5–5 mg mL^{-1}) enhance the PLQY due to surface defect passivation and improve the PeLEDs in terms of operational stability[37,38] while higher polymer percentages result in higher PeLED efficiencies (EQE).[13,30] In all published works, although the role of the polymer percentage in controlling nucleation and growth of MHPs grains has been suggested[39] the detailed interaction mechanism is not fully understood due to the chemical complexity of the solution containing the MHPs precursors.

Among the wide variety of existing polymers, cellulose is pointed out as the best option for designing eco-friendly devices due to their unique chemical and structural properties.[40,41] However, only a few articles report the use of cellulose in combination with MHPs for energy and electronics applications.[42–44] For example, very low incorporation of cellulose (0.01–1 mg mL^{-1} or 0.001–0.1 wt.%) into a 3D $MAPbI_3$ perovskite layer has proved to enhance the operation stability and efficiency of PSCs devices.[45–47]

Herein, we report the use of a mostly based β-(1,4) cellulose oligosaccharide (COS) to control the formation of nanocrystals of the $BA_2MA_4Pb_5I_{16}$ (BA = *n*-butylammonium and MA = methylammonium) 2D Ruddlesden-Popper (RP) hybrid perovskite for light-emitting applications. In this work, the increasing content of COS (0.3–20 wt.% or 1–75 mg mL^{-1}) in PeLEDs enhances both the operational stability (T_{50} = 0.5 min. without COS vs T_{50} = 10 min. with 75 mg mL^{-1} of COS, T_{50} is the time at which the efficiency of the PeLEDs reduces to half of the initial value) and the performance (a six-fold increase of luminance). The enhanced stability is ascribed to a protective effect against moisture and O_2 of the COS compound and the suppression of high leakage current due to the better quality and homogeneity of the films containing the COS compound. The higher luminance is explained due to the larger PLQY of the 2D RP perovskite films with the COS compound, as a result of a larger exciton binding energy, E_b. The SEM images and the analysis of the width of the X-ray diffraction (XRD) peaks reveal a reduction of the grain size to the nanometer scale, consistent with the rise of the E_b due to spatial confinement.

2. Results

The synthetic cellulose oligosaccharide (COS) was obtained from the mechanocatalytic depolymerization of cellulose. Further details related to its obtention and characterization are described in the Supporting Information . The incorporation of the COS compound into the 2D RP $BA_2MA_4Pb_5I_{16}$ hybrid perovskite films is performed through its addition to the MHPs precursor solutions. Thus, BAI, MAI, and PbI_2 in a 2:4:5 molar ratio are dissolved in DMF at 0.6 M (PbI_2) followed by the addition of COS at different concentrations (1, 5, 10, 25, 50, and 75 mg mL^{-1}). The stoichiometric ratio of the precursors in the solution only defines the canonical formula for the 2D RP perovskite, $BA_2MA_4Pb_5I_{16}$, but a mixture of different phases (variation of the number of octahedra layers) is always obtained for the 2D RP perovskites. The thin films were prepared by the spin-coating technique obtaining blended films of the 2D RP $BA_2MA_4Pb_5I_{16}$ perovskite and the cellulose oligosaccharide (**Figure 1**a), see the supporting information for details.

The changes in the crystalline structure of the 2D RP perovskite films caused by the COS have been investigated by using X-ray diffraction (XRD) at Cu K_α wavelength (1.54 Å). In Figure 1b,c, the XRD diffractograms of the films exhibit two XRD peaks at 14.07° and 28.37°, which are typically assigned to the (111) and (202) crystallographic planes of the 2D perovskites.[48] However, the XRD peaks are broadened at high COS concentrations, 50 and 75 mg mL^{-1}, suggesting a reduction in the size of the crystalline domains. The mean size of the domains was calculated using the Scherrer equation,[49] which showed a symmetrical three-fold reduction of the mean size of the crystallites from ≈110 nm to ≈40 nm at high COS percentage (Figure S2, Supporting Information). This indicates the formation of 2D RP perovskite nanocrystals (NCs) incorporation of a very low concentration e.[50]

The orientation of the perovskite domains is a key factor that determines the vertical conductivity of the 2D RP perovskites for optoelectronic applications. Synchrotron Grazing Incident Wide Angle X-ray Scattering (GIWAXS) measurements at ALBA synchrotron (Cerdanyola, Spain) were performed to analyze the changes in the orientation of the blended films depending on the COS concentration (Figure 1d). Thanks to the grazing incidence configuration, the sample was probed over a larger beam footprint compared to the transmission mode, obtaining average statistical information of the sample. GIWAXS results showed that without COS added (0 mg) the perovskite films exhibit a typical scattering texture with multiple bright small diffraction spots, indicating a high crystalline orientation of large crystals of the 2D RP perovskite. At low COS content (10 mg mL^{-1}) the spots are transformed into narrow bands, but still contain bright regions, revealing a texturization of the perovskite and hence, losing the initial well-oriented structure. At high COS content (50

E. Solano
NCD-SWEET Beamline
ALBA Synchrotron Light Source
Cerdanyola del Vallès
Barcelona 08290, Spain
D. Hermida-Merino
CINBIO
Departamento de Física Aplicada
Universidade de Vigo
Campus Lagoas-Marcosende
Vigo 36310, Spain

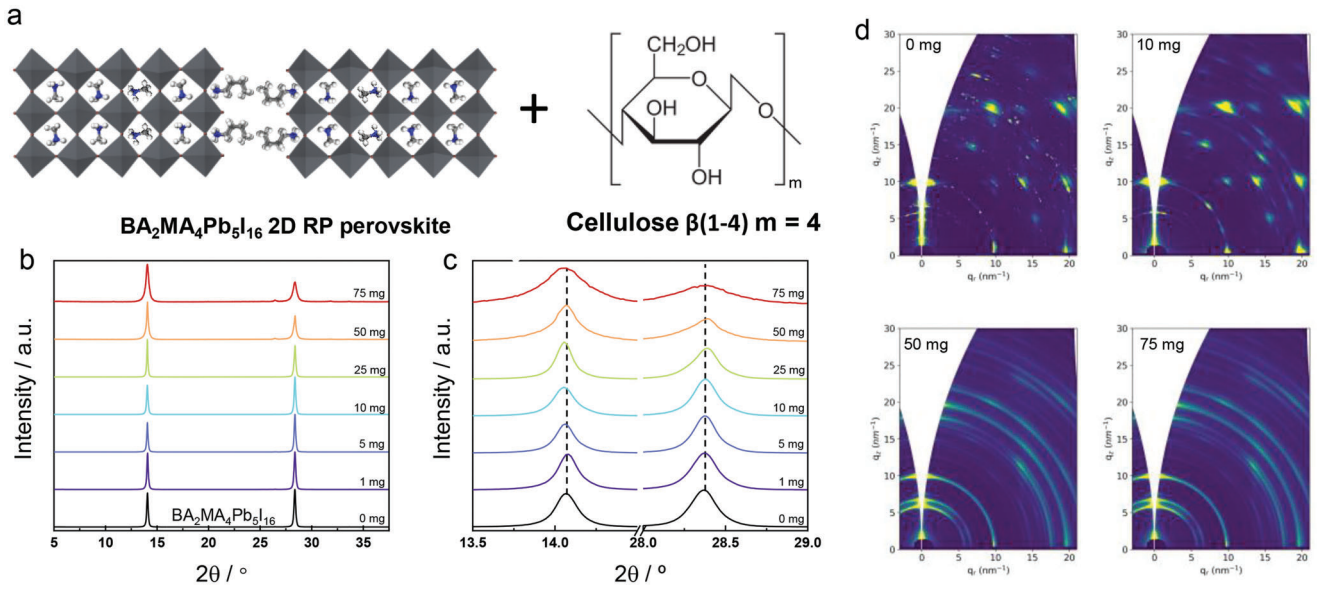

Figure 1. Structure and orientation of the blended COS/2D RP perovskite films. a) Schematic illustration of the chemical structure of the 2D RP perovskite and the cellulose oligosaccharide b,c) Normalized X-ray diffraction (XRD) patterns recorded at Cu K_α wavelength (1.54 Å) (b) and magnification of the reflection peaks (c) of the $BA_2MA_4Pb_5I_{16}$ 2D RP perovskite films blended with different amount of the COS in the initial precursor solution: 0, 1, 5, 10, 25, 50, and 75 mg mL^{-1}. d) 2D GIWAXS patterns of the $BA_2MA_4Pb_5I_{16}$ 2D RP perovskite films containing different amounts of the COS in the initial precursor solution: 0, 10, 50, and 75 mg mL^{-1}.

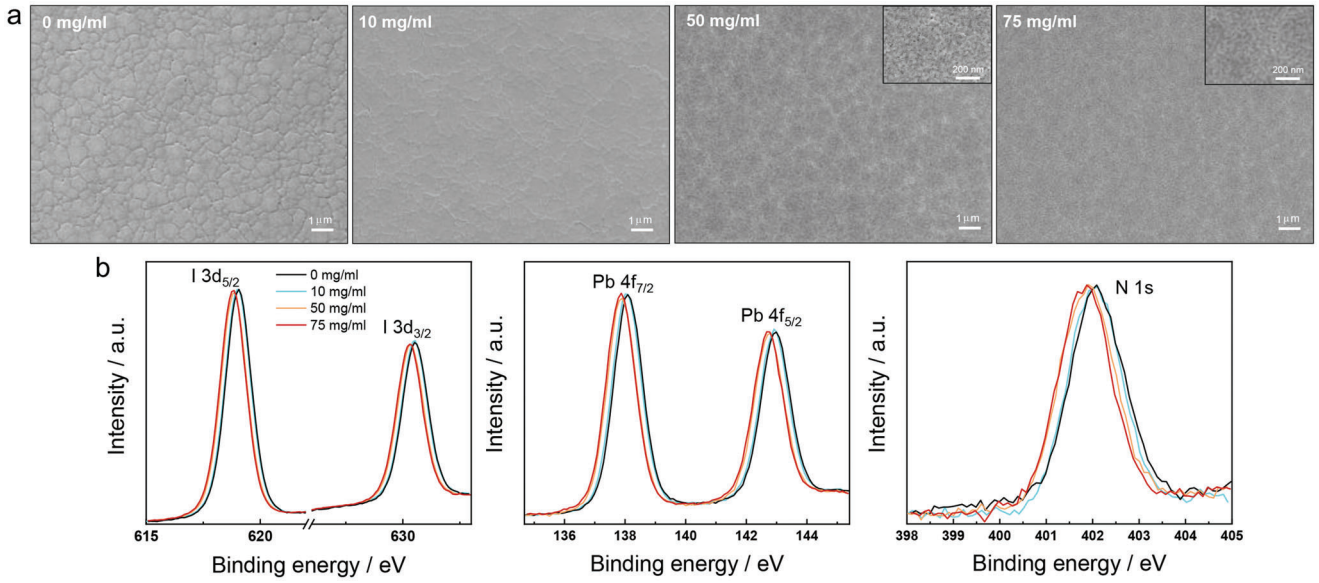

Figure 2. Morphology and interactions of the blended COS/2D RP perovskite films. a) Top-surface SEM images of the 2D RP perovskite films containing 0, 10, 50, and 75 mg mL^{-1} of the COS compound. Scale bar = 1 μm and 200 nm (inner image) b) XPS spectra of I 3d, Pb 4f, and N 1s of the $BA_2MA_4Pb_5I_{16}$ 2D RP perovskite films containing 0 mg mL^{-1} (black line), 10 mg mL^{-1} (blue line), 50 mg mL^{-1} (orange line), and 75 mg mL^{-1} (red line) of the cellulose oligosaccharide.

and 75 mg mL^{-1}), the disorientation effect is more pronounced, resulting in a quasi-isotropic sample with almost no preferential orientation. Also, band broadening indicates a reduction of the crystallite size. Thus, the intercalation of the COS compound within the 2D RP perovskite domains also hampers the functioning of the template effect that produces the preferential growth of certain crystallographic planes within the films and the reduction of the crystal domain size.

To characterize the influence of the COS on the size and morphology of the 2D RP perovskite NCs, Scanning Electron Microscopy (SEM) was performed. **Figure 2**a illustrates the top-surface images of the different films displaying significant

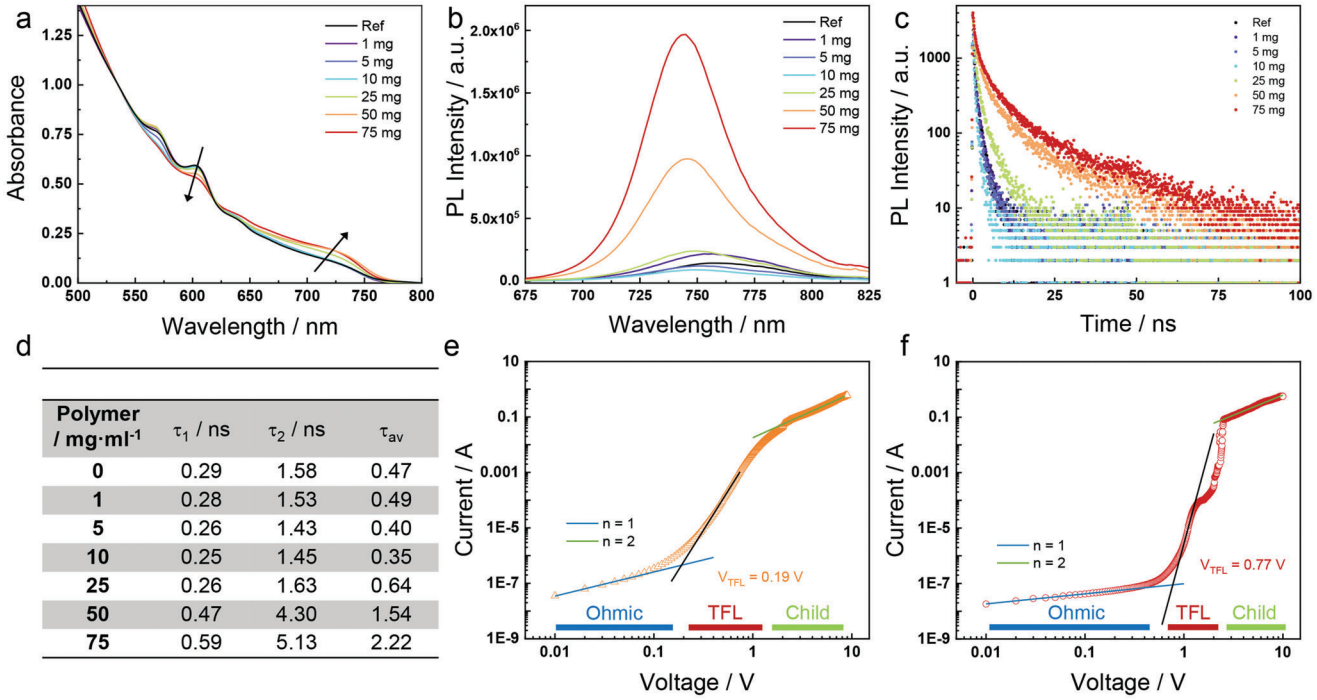

Polymer / mg·ml^{-1}	τ_1 / ns	τ_2 / ns	τ_{av}
0	0.29	1.58	0.47
1	0.28	1.53	0.49
5	0.26	1.43	0.40
10	0.25	1.45	0.35
25	0.26	1.63	0.64
50	0.47	4.30	1.54
75	0.59	5.13	2.22

Figure 3. Spectroscopic characterization of the blended COS/2D RP perovskite films. a–c) UV–vis absorption spectra (a), photoluminescence, PL, spectra (b) and time-resolved PL decays of the BA2MA4Pb5I16 2D RP perovskite films with different amounts of the COS compound in the initial precursor solution: 0, 1, 5, 10, 25, 50, and 75 mg mL^{-1}. λexc = 405 nm. d) PL lifetimes derived from a biexponential fit of the experimental data displayed in panel (c). e,f) Dark *J–V* curves for electron-only devices of the BA2MA4Pb5I16 2D RP perovskite films containing 0 mg/mL (e) and 75 mg mL^{-1} (f) of the COS compound.

variations upon increasing the COS percentage. In the films without COS or at low COS content, the SEM images display a compact film with a flat surface formed by a densely packed grain structure with a grain size range from 200 to 700 nm. The observed size of the grains mismatch with the crystallite size (≈110 nm) calculated from the XRD measurements which indicates that a large majority of the grains are composed of many crystallites.[6] These results are in agreement with the 2D GIWAXS patterns recorded since the presence of highly oriented and big grains was deduced from the scattering patterns. On the other hand, at high COS percentages (50 and 75 mg mL^{-1}), the size of the grains is considerably reduced leading to a very homogeneous film, but as observed with GIWAXS, highly textured. A higher magnification of the SEM image exhibits clusters of grains with an average size of 30–40 nm, matching well with that deduced from the width of the XRD peaks. These results are relevant since they clearly prove that the addition of high COS content reduces the size of the 2D RP domains to the nanometer scale.

To investigate the type of interactions between the surface of the grains of the 2D RP perovskite and the functional groups of the COS compound, X-ray photoelectron spectroscopy (XPS) measurements were carried out. Figure 2b illustrates the XPS spectra of I 3d, Pb 4f, and N 1s for the 2D RP perovskite films with a COS content of 0, 10, 50, and 75 mg mL^{-1}. Interestingly, the XPS signal of the three atoms, I, Pb, and N, display the same shift to lower binding energy, being more intense in the films containing 50 and 75 mg mL^{-1} of the COS compound. The shift to lower binding energies can be explained due to the close proximity of the electronegative O atoms present in the COS compound to the surface of the 2D RP perovskite grains which produces an increased electron cloud density around the Pb, I and N atoms.[51,52,53] The previous result demonstrates the interaction between both the COS compound and the surface of the 2D RP perovskite grains. Additionally, FTIR measurements were performed to further investigate the formation of specific chemical interactions in both materials. Figure S3 (Supporting Information) displays a broad and intense FTIR signal centered at 3321 cm^{-1} in the film of the COS compound due to O–H stretch vibration modes, which indicates the formation of intra- and intermolecular H-bonds. In the FTIR spectra of the blended COS/2D RP perovskite films, the signal of the O–H stretch vibration modes is shifted to a higher wavenumber and with a similar width of the peaks. This fact indicates that new types of H-bonds are formed in the presence of the 2D RP $BA_2MA_4Pb_5I_{16}$ perovskite, which proves the formation of specific interactions between both materials in the films.

The optical properties of the $BA_2MA_4Pb_5I_{16}$ 2D RP perovskite were studied by using steady-state and time-resolved absorption and photoluminescence (PL) spectroscopy at different COS percentages. **Figure 3**a exhibits the absorption spectra for the 2D RP perovskite showing three excitonic absorption bands ≈570, 605, and 640 nm and the absorption onset at 750 nm. In 2D RP perovskites, the high-energy absorption bands are attributed to the formation of excitons due to quantum confinement in the inorganic layers whose thickness is represented by the *n* value,

i.e., number of octahedra layers.[54,55] Thus, the observed absorption peaks are assigned to the $n = 2$, 3, and 4 phases from the high- to low-energy absorption bands, respectively. As displayed in Figure 3a, the COS addition modifies the distribution of the n phases in the film, decreasing the content of the low dimensional phases ($n = 2$ and 3) and increasing the absorption at red-shifted wavelengths (700–745 nm) with respect to the absorption onset. In line with this observation, the normalized PL spectrum (Figure S3a, Supporting Information) exhibits a gradual blue shift upon increasing the COS percentage in the films (λ_{max} = 760 to 745 nm at 75 mg mL^{-1}). Moreover, the weak PL signal from the low dimensional phases (Figure S3b, Supporting Information) practically vanishes at high COS content. These results prove a change in the phase distribution due to COS addition. The phases with a large stacking of inorganic layers ($n \approx \infty$) are not formed but only those with finite n values ($n = 7$–10).[56] Thus, in addition to the decrease in the size of the 2D RP perovskite grains, the COS content in the films controls the growth of the number of octahedra layers in the grains.

Regarding the PL measurements, Figure 3b displays the PL spectra of the $BA_2MA_4Pb_5I_{16}$ 2D RP perovskite at increasing content of the COS compound. The addition of a moderate amount of COS (1–25 mg mL^{-1}) only slightly modifies the intensity of the PL signal. However, at high COS content, 50–75 mg mL^{-1}, an up to 14-fold increase in the PL signal is observed. This result is remarkable since the vast majority of the reported studies display a moderate rise of the PL signal when adding a polymer additive into the perovskite films.[13,35,37,38] Surface passivation is generally described as the mechanism responsible for the modest increase in PL but, in our samples, the significant rise of the PL indicates an alternative origin for this experimental result. The measured PLQY of the film with 75 mg mL^{-1} of the COS compound is 12% at a very low excitation intensity of 1 mW cm^{-2} which is a notable value for a 2D RP perovskite film with *n*-butylammonium as the large organic cation.[57,58] Time-resolved PL measurements reveal a similar trend. While slightly similar time decays are observed at low COS content (< 25 mg mL^{-1}), a significant elongation of the PL decays is observed at high COS content, 50 and 75 mg mL^{-1} (Figure 3c). Table in figure 3d collects the time decays after fitting the experimental data with bi-exponential functions. The average time decays are also displayed in Table in figure 3d. The longer values for the time decays in the films with high COS content are in line with the larger PLQYs of these films. The usual justification found in the literature for the moderate increase in PLQY after polymer doping of MHPs films is surface passivation of defects.[59,60] However, the intense rise of the PLQY in our films with high COS content must be accounted for other additional mechanisms, such as size-dependence effects or delayed fluorescence.[61,62]

To get an insight into the mechanism, the determination of defect concentration in the MHPs films upon variation of the COS percentage has been carried out. In this regard, the space charge limited current (SCLC) method in single carrier devices (electron or hole only devices) allows one to calculate the defect concentration by measuring trap densities (N_t) from the voltage at the trap-filling limited (TFL) region.[63–65] Figure 3e,f and **Figures** S4,S5 (Supporting Information) display the dark *J*–*V* curves for electron- and hole-only devices of the $BA_2MA_4Pb_5I_{16}$ 2D RP perovskite films at different COS concentrations. In the film without the COS compound, the obtained N_t values, $N_{CBM} = 10^{16}$ cm^{-3} and $N_{VBM} = 10^{15}$ cm^{-3}, are in good agreement with those reported in the literature for 2D perovskite films.[66,67] Similarly to the PL measurements, the defect concentration barely changes at moderate COS percentage (10 mg mL^{-1}) while it rises, especially for defects close to the CBM, at high content of the COS compound ($N_{CBM} = 4 \cdot 10^{16}$ cm^{-3} and $N_{VBM} = 2 \cdot 10^{15}$ cm^{-3}). The reason behind of the higher surface trap density can be ascribed to the mentioned reduction of the crystalline size (XRD data) which dramatically increases the specific surface area in the blended films with high COS percentage. These outcomes certainly rule out the role of the COS compound as a passivating agent of the surface defects in the 2D RP perovskite. It has been reported that the high PLQY of MHPs is due to a rapid reversible process of multiple trapping and de-trapping of carriers from deep traps.[68] In this sense, the observed increased concentration of defects close to the bands in our films might stimulate the spontaneous radiative recombination of the carriers after de-trapping, explaining the higher PLQY and longer PL time decays.

The transport and recombination mechanism of the photogenerated charges in the 2D RP perovskites was studied by using femtosecond transient absorption spectroscopy. Figure S6 (Supporting Information) displays the transient spectra at different pump-probe delays. Photobleaching bands at 570, 610, and 640 nm are observed at early times for all films which are assigned to the $n = 2$, 3, and 4 phases, while at longer times, a broad bleaching signal at 730 nm appears which is associated to phases with high n values. Figure S7 (Supporting Information) shows that the different photobleaching signals evolve on distinct timescales, with a concomitant decay of the transient signals with low n values and a growth of the signals with high n values. This behavior is typically reported for a downward funneling of energy of the photogenerated charges in phases with low n values to those featuring high n values.[58] This energy cascade is almost complete after ≈100 ps and then, the recombination dynamics take place from the phase with the highest n value. Figure S8 (Supporting Information) displays a small blue shift of the transient absorption spectra measured after a 200 ps delay for films with increasing COS percentage, which is consistent with an increased proportion of phases with moderate n values ($n = 7$–10) as it was observed in the steady-state absorption and PL measurements. Importantly, the same recombination kinetics in all thin films highlights that the addition of the COS compound does not alter the initial ultrafast energy transfer from lower to higher dimensional phases in the 2D RP perovskites.

To further investigate the origin of the high PLQY in films with high COS content, temperature dependence PL measurements were performed. **Figure 4**a,b, and Figure S9 (Supporting Information) exhibit the PL spectra of the $BA_2MA_4Pb_5I_{16}$ 2D RP perovskite films at different COS concentrations from 300 to 80 K. It is observed a continuous blue shift of the PL signal at increasing temperatures in all films which is a counterintuitive result compared to most known semiconductors.[69,70] The competition between thermal expansion and electron-phonon interactions is the mechanism responsible for the temperature evolution of the band gap (renormalization) and therefore, the position of the PL band.[71,72] A closer view to the PL signals reveals certain asymmetry (a weak shoulder at lower energy) in the shape of the bands which has been attributed to two emission

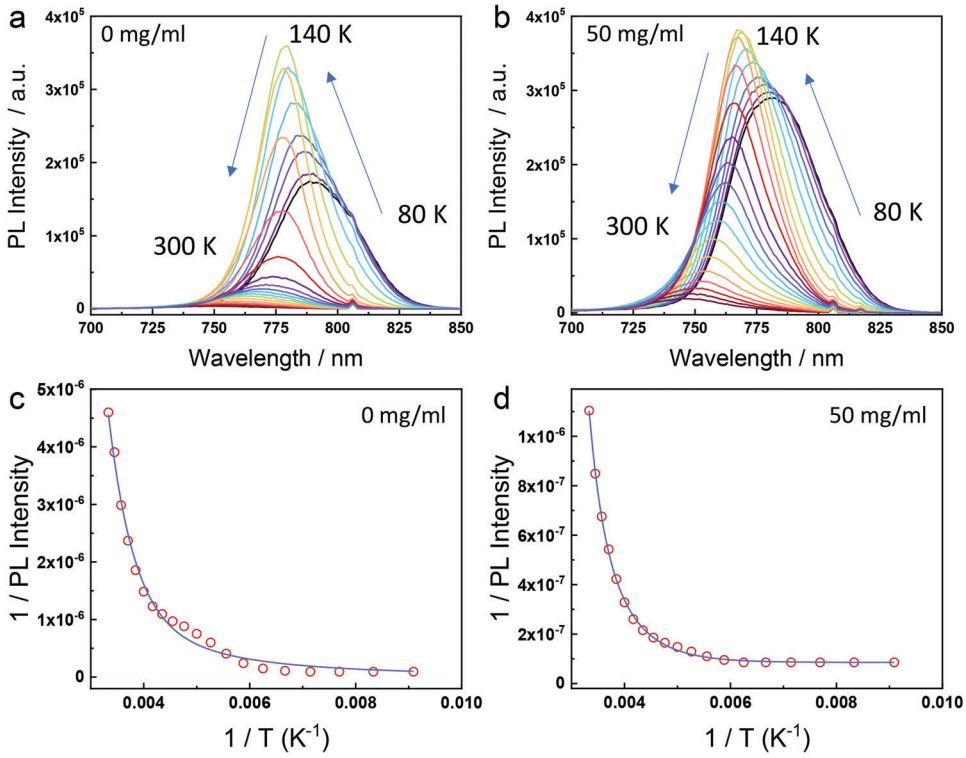

Figure 4. Calculation of the exciton binding energy, E_b. a,b) Photoluminescence spectra of the $BA_2MA_4Pb_5I_{16}$ 2D RP perovskite films at different temperatures (80–300 K) containing 0 mg mL^{-1} a) and 50 mg mL^{-1} b) of the COS compound. c,d) 1/Integrated PL intensity as a function of 1/T of the $BA_2MA_4Pb_5I_{16}$ 2D RP perovskite films containing 0 mg mL^{-1} (c) and 50 mg mL^{-1} (d) of the COS compound. The solid lines are best fits using a model that assumes the existence of free and self-trapped excitons.

peaks from free excitons (charges) and self-trapped states.[73] The FWHM of the temperature dependence PL peaks are collected in Table S1 (Supporting Information), where a narrowing of the peak is observed ≈160 K in both samples. To investigate the changes in the relaxation dynamics of the 2D RP perovskites upon COS addition, the temperature dependence PL intensity was quantitatively analyzed. In the low-temperature regime, 140–80 K, the PL intensity decreases as the temperature drops which is generally explained due to thermal escape of trapped carriers in the interfacial states.[69] In the high-temperature regime, 150–300 K, the PL intensity is reduced as the temperature increases due to exciton dissociation and trapping in surface defects or ion vacancies.[74] The experimental PL data at the high-temperature regime are employed to estimate the exciton binding energy for the different blended films. Equation (1) expresses the variation of PL intensity (I_{PL}) versus temperature[74]

$$\frac{1}{I_{PL}(T)} = \frac{1}{I_0} + Be^{-E_a/(kT)} + Ce^{-E_b/(kT)} \quad (1)$$

Where I_0 is the PL intensity at 0 K, B, and C are preexponential factors, E_b is the exciton dissociation or exciton binding energy, E_a is the activation energy for thermal de-trapping and k_B is the Boltzmann constant.[75] Figure 4c,d and Figure S9 (Supporting Information) represent the inverse of the integrated PL intensity of the 2D RP perovskite in the blended films as a function of $1/T$. It is observed that the decrease in the PL intensity occurs at lower temperatures in the films without COS or with a low percentage (10 mg Ml^{-1}) as a result of a lower binding energy. Fitting the PL traces with equation (1) resulted in particularly different exciton binding energies, E_b, for the films. Thus, a value of $E_b = 180$ meV was obtained for the film without the COS compound. The reported E_b value for a pure-phase ($n = 5$) and for a mixed-phase ($n = 4$) BA-based 2D RP perovskite is in the range of 100–220[76,77] and 242[70] meV, respectively. The obtained E_b values for the films with a high COS content (50 and 75 mg mL^{-1}) rise to 350 and 370 meV. In these blended films, the low dimensional phases ($n = 2$ and 3) with high E_b values are strongly reduced, so that the increase in E_b cannot be assigned to the change in phase distribution. Thus, in line with the three-fold reduction of the mean size of the crystallites at a high COS percentage determined from the XRD measurements, the increase of the E_b can be related to a spatial confinement effect generated in the nanometer-scale perovskite grains. The high value of E_b in the films with a high percentage of the COS compound prevents the dissociation of the excitons into a free charge carrier, enhancing the radiative deactivation and, therefore, the probability of PL emission.[78] The high PLQY in the films with high COS content is then ascribed to both a delayed fluorescence caused by the higher amount of defects, and an efficient radiative recombination of the photogenerated excitons due to spatial confinement.

To explore additional beneficial effects of adding high content of COS to the 2D RP perovskites, the stability of the films was tested. The blended films were stored under environmental

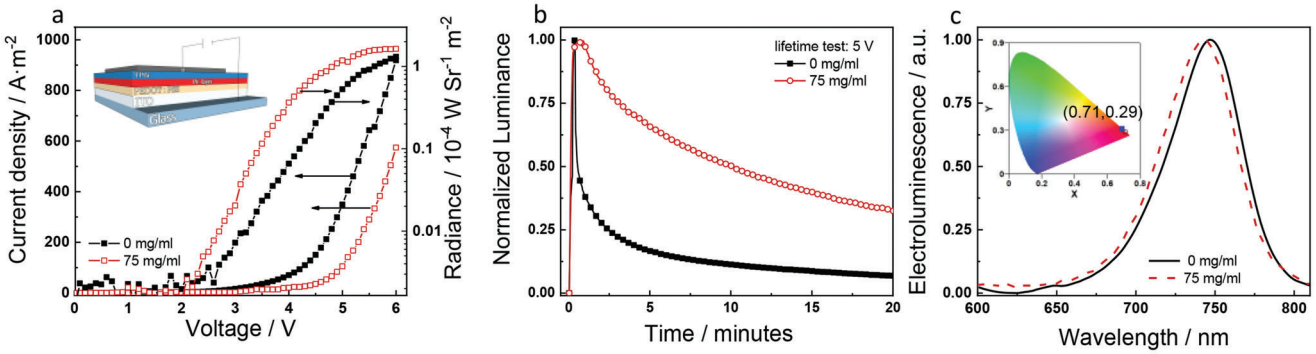

Figure 5. Characterization of the PeLEDs. a–c) Current density-voltage and radiance curves (a), radiance stability test (b), and electroluminescence spectra (c) of the $BA_2MA_4Pb_5I_{16}$ 2D RP perovskite light emitting device containing 0 mg mL^{-1} (black line) and 75 mg mL^{-1} (red line) of the COS compound.

conditions at room temperature for more than three months. The photographs of both 2D RP perovskite films w/o COS (Figure S10, Supporting Information) reveal a clear enhancement of the stability at a glance. While the film without COS appears yellowish because of prompt degradation of the material to the PbI_2 precursor, the color is brownish in the films containing the COS compound, as in the freshly prepared films. The 2D scattering patterns from GIWAXS confirm the better stability of the films with COS (Figure S11, Supporting Information). A clear evolution towards a more textured and oriented crystalline structure was evident (smaller and brighter Bragg peaks) for the parent and low COS content (10 mg mL^{-1}) films, while in samples with 50 mg mL^{-1} and 75 mg mL^{-1} of COS, the preferential orientation is almost unaltered (noticed by the anisotropic diffraction rings). In order to clarify the higher stability of the crystalline structure against aging, azimuthal χ (2D) cuts patterns at |q| 10 and 20 nm^{-1} were done, showing the intensity profiles along the different azimuthal χ exiting angles (Figure S12, Supporting Information). While the film without COS compound clearly presents a variation of the scattering peak positions, the films with the COS compound, which presented a polycrystalline isotropic structure, retained a similar scattering pattern after three months. Therefore, COS provides superior resistance toward moisture inhibiting the typical degradation reactions in MHPs (i.e.,. defect formation, phase separation).[79]

Based on the enhanced optical properties and the excellent stability of the blended films, the fabrication of perovskite light emitting devices (PeLEDs) by adding COS in the electroluminescent 2D RP perovskite film was examined. The inset of **Figure 5**a shows the architecture for the "proof-of concept" devices. In both devices (without COS and with 75 mg Ml^{-1} of COS), bright light PeLED devices with high color purity (CIE coordinates 0.71, 0.29) were obtained with an almost unchanged position with respect to their PL spectra (Figure 5c). Figure 5a illustrates the current density and luminance expressed as a radiance of both devices. While a higher turn-on voltage (5 V instead of 4 V) and a 3-fold reduction in the current density were observed when the COS compound is present, a six-fold increase of luminance (from $1.9{\cdot}10^{-5}$ to $\approx 1.18{\cdot}10^{-4}$ W Sr m^{-2}, at 5 V) was also obtained. These outcomes clearly prove that the 2D RP perovskite is responsible for the electroluminescence in both devices and the presence of the COS compound improves the PeLEDs performance by increasing the luminance. The reduction of the current density in the PeLEDs can be ascribed to the low conductivity of the COS compound while the enhanced luminance can be related to both reduction of the non-radiative recombination along grain boundaries interfaces[80] and efficient radiative recombination due to spatial confinement in the nanometer-scale grains.

Since the stability of the MHPs under operation in a device is the major drawback of the PeLEDs, the luminance of non-encapsulated devices was tested at a fixed current density (200 A m^{-2}, 5 V) inside an N_2-filled globe box (Figure 5b). While the device without COS has a T_{50} (operational lifetime to reach 50% of the initial luminance) of 0.5 min, $T_{50} = 10.0$ min (20 times better) was obtained for the device prepared with 75 mg mL^{-1} of COS. Since moisture and O_2 are the most common extrinsic factors to degrade the MHPs,[67,81] the COS compound is expected to act as a protective scaffold against those agents. However, the COS compound also induces the formation of smaller crystal size, high quality and homogeneous films, both factors directly involved in the stability of the devices. The reason behind this is the suppression of high leakage current in the pinhole-rich perovskite films, mainly caused by the presence of grain boundaries in large crystals.[82]

3. Conclusion

The addition of a large amount of polymer additives to MHPs layers has not been studied in depth in the literature. Our work proves the two-fold behavior during the addition of the COS compound to the 2D RP perovskite films. A reduced content of COS in the films, between 1 and 25 mg mL^{-1}, does not produce major changes in the structure, orientation, morphology, defect concentration, or optical properties of the $BA_2MA_4Pb_5I_{16}$ 2D RP perovskite film. This result is in line with previous reports where PeLEDs fabricated with this approach only display a moderate improvement in stability. However, the increased content of COS to 50–75 mg mL^{-1} in the films notably modifies their size and texture, changing the optoelectronic features of the film. In particular, the high content of COS is homogeneously intercalated among the perovskite grains reducing its size to the nanometer scale (30–40 nm), close to the quantum confinement scale. Indeed, both the higher PLQY (14-fold) and longer PL decays are attributed to the decrease of grain size that entails a rise of the

exciton binding energy, E_b (370 meV in films with 75 mg Ml^{-1} of the COS compound) as measured with temperature dependence PL measurements. The fabricated PeLEDs containing high COS content display both enhanced luminance and stability. The origin of the large luminance in the PeLEDs is the more efficient radiative deactivation of the excitons (large E_b) and the reduction of the non-radiative recombination along grain boundary interfaces since the films are more homogenous. Regarding the enhanced operational stability, the COS compound acts as a protecting scaffold against moisture and O_2 but also promotes the decrease of grain boundaries (smaller crystals) which suppress the leakage current that degrades the structure of the MHPs.

Our work may pave the way for investigating other types of polymer additives at high concentrations blended in MHPs films for optoelectronic devices. The nature of the functional groups present in the polymer is expected to regulate the interactions between both materials and, therefore, the morphology and optical properties of the blended film. In addition, the selected polymer must also fulfill the requirements needed for high-efficient PeLEDs devices.

Supporting Information

Supporting Information is available from the Wiley Online Library or from the author.

Acknowledgements

S.R.-T. thanks the Ministry of Universities for a FPU fellowship (FPU18/04452). The authors gratefully acknowledge the financial support: PID2020-119209RB-I00 and PID2021-128761OA-C22 project grants funded by MCIN/AEI/10.13039/501100011033 by "ERDF A way of making Europe". This research was also supported by the Andalusian Government through the PY20_01151 project. The SBPLY/21/180501/000127 project was funded by JCCM and by the EU through "Fondo Europeo de Desarollo Regional" (FEDER). GIWAXS experiments were performed at NCD-SWEET beamline at ALBA Synchrotron with the collaboration of ALBA staff and with the grant no. 2022035803. P.G.A., L.S., H.C., and S.L. acknowledge the Centre National de la Recherche Scientifique, the Région Nouvelle Aquitaine, and the Université de Bordeaux. F.J. is thankful to the Université de Poitiers. D.H.M acknowledge the funding from the Ministerio de Universidades (budget implementation 33.50.460A.752) and the European Union NextGenerationEU/PRTR through the Maria Zambrano contract of the University of Vigo. Funding for open access charge: Universidad de Córdoba/CBUA

Conflict of Interest

The authors declare no conflict of interest.

Data Availability Statement

The data that support the findings of this study are available from the corresponding author upon reasonable request.

Keywords

cellulose, hybrid materials, metal halide perovskites, nanocrystals, perovskite light emitting diodes, polymer additives

Received: March 21, 2023
Revised: May 31, 2023
Published online: July 14, 2023

[1] M. Jeong, I. W. Choi, E. M. Go, Y. Cho, M. Kim, B. Lee, S. Jeong, Y. Jo, H. W. Choi, J. Lee, J. H. Bae, S. K. Kwak, D. S. Kim, C. Yang, *Science* **2020**, *369*, 1615.
[2] D. I. Kim, J. W. Lee, R. H. Jeong, J. H. Boo, *Sci. Rep.* **2022**, *12*, 697.
[3] K. Liu, Y. Luo, Y. Jin, T. Liu, Y. Liang, L. Yang, P. Song, Z. Liu, C. Tian, L. Xie, Z. Wei, *Nat. Commun.* **2022**, *13*, 4891.
[4] C. Chen, J. Chen, H. Han, L. Chao, J. Hu, T. Niu, H. Dong, S. Yang, Y. Xia, Y. Chen, W. Huang, *Nature* **2022**, *612*, 266.
[5] C. Sun, Y. Zhang, C. Ruan, C. Yin, X. Wang, Y. Wang, W. W. Yu, *Adv. Mater.* **2016**, *28*, 10088.
[6] H. Cho, S. H. Jeong, M. H. Park, Y. H. Kim, C. Wolf, C. L. Lee, J. H. Heo, A. Sadhanala, N. S. Myoung, S. Yoo, S. H. Im, R. H. Friend, T. W. Lee, *Science* **2015**, *350*, 1222.
[7] W. Chen, M. Zhou, Y. Liu, X. Yu, C. Pi, Z. Yang, H. Zhang, Z. Liu, T. Wang, J. Qiu, S. F. Yu, Y. Yang, X. Xu, *Adv. Funct. Mater.* **2022**, *32*, 2107424.
[8] S. Yakunin, M. Sytnyk, D. Kriegner, S. Shrestha, M. Richter, G. J. Matt, H. Azimi, C. J. Brabec, J. Stangl, M. V. Kovalenko, W. Heiss, *Nat. Photonics* **2015**, *9*, 444.
[9] B. Jeong, L. Veith, T. J. A. M. Smolders, M. J. Wolf, K. Asadi, *Adv. Mater.* **2021**, *33*, 2100486. .
[10] W. Yu, F. Li, L. Yu, M. R. Niazi, Y. Zou, D. Corzo, A. Basu, C. Ma, S. Dey, M. L. Tietze, U. Buttner, X. Wang, Z. Wang, M. N. Hedhili, C. Guo, T. Wu, A. Amassian, *Nat. Commun.* **2018**, *9*, 5354.
[11] S. Yakunin, L. Protesescu, F. Krieg, M. I. Bodnarchuk, G. Nedelcu, M. Humer, G. De Luca, M. Fiebig, W. Heiss, M. V. Kovalenko, *Nat. Commun.* **2015**, *6*, 8056.
[12] C. Y. Huang, C. Zou, C. Mao, K. L. Corp, Y. C. Yao, Y. J. Lee, C. W. Schlenker, A. K. Y. Jen, L. Y. Lin, *ACS Photonics* **2017**, *4*, 2281.
[13] W. Cai, Z. Chen, Z. Li, L. Yan, D. Zhang, L. Liu, Q. H. Xu, Y. Ma, F. Huang, H. L. Yip, Y. Cao, *ACS Appl. Mater. Interfaces* **2018**, *10*, 42564.
[14] Y. Jiang, C. Qin, M. Cui, T. He, K. Liu, Y. Huang, M. Luo, L. Zhang, H. Xu, S. Li, J. Wei, Z. Liu, H. Wang, G. H. Kim, M. Yuan, J. Chen, *Nat. Commun.* **2019**, *10*, 1868.
[15] L. Xu, J. Li, B. Cai, J. Song, F. Zhang, T. Fang, H. Zeng, *Nat. Commun.* **2020**, *11*, 3902.
[16] B. Han, S. Yuan, T. Fang, F. Zhang, Z. Shi, J. Song, *ACS Appl. Mater. Interfaces* **2020**, *12*, 14224.
[17] S. Li, Y. Wu, C. Zhang, Y. Liu, Q. Sun, Y. Cui, S. F. Liu, Y. Hao, *ACS Appl. Mater. Interfaces* **2020**, *12*, 45073.
[18] A. Liu, C. Bi, R. Guo, M. Zhang, X. Qu, J. Tian, *Adv. Opt. Mater.* **2021**, *9*, 2002167.
[19] M. H. Park, S. H. Jeong, H. K. Seo, C. Wolf, Y. H. Kim, H. Kim, J. Byun, J. S. Kim, H. Cho, T. W. Lee, *Nano Energy* **2017**, *42*, 157.
[20] J. S. Kim, J.-M. Heo, G.-S. Park, S.-J. Woo, C. Cho, H. J. Yun, D.-H. Kim, J. Park, S.-C. Lee, S.-H. Park, E. Yoon, N. C. Greenham, T.-W. Lee, *Nature* **2022**, *611*, 688.
[21] M. Xie, J. Tian, *J. Phys. Chem. Lett.* **2022**, *13*, 1962.
[22] Y. H. Kim, H. Cho, J. H. Heo, T. S. Kim, N. S. Myoung, C. L. Lee, S. H. Im, T. W. Lee, *Adv. Mater.* **2015**, *27*, 1248.
[23] Z. K. Tan, R. S. Moghaddam, M. L. Lai, P. Docampo, R. Higler, F. Deschler, M. Price, A. Sadhanala, L. M. Pazos, D. Credgington, F. Hanusch, T. Bein, H. J. Snaith, R. H. Friend, *Nat. Nanotechnol.* **2014**, *9*, 687.
[24] Y. H. Kim, H. Cho, T. W. Lee, *Proc. Natl. Acad. Sci. USA* **2016**, *113*, 11694.

[25] X. Liu, N. Zhang, B. Tang, M. Li, Y. W. Zhang, Z. G. Yu, H. Gong, *J. Phys. Chem. Lett.* **2018**, *9*, 5862.
[26] Y. Rong, L. Liu, A. Mei, X. Li, H. B. E. Han, *Adv. Energy Mater.* **2015**, *5*, 1501066.
[27] D. Bryant, N. Aristidou, S. Pont, I. Sanchez-Molina, T. Chotchunangatchaval, S. Wheeler, J. R. Durrant, S. A. Haque, *Energy Environ. Sci.* **2016**, *9*, 1655.
[28] T. H. Han, J. W. Lee, C. Choi, S. Tan, C. Lee, Y. Zhao, Z. Dai, N. De Marco, S. J. Lee, S. H. Bae, Y. Yuan, H. M. Lee, Y. Huang, Y. Yang, *Nat. Commun.* **2019**, *10*, 520.
[29] S. Yuan, L. S. Cui, L. Dai, Y. Liu, Q. W. Liu, Y. Q. Sun, F. Auras, M. Anaya, X. Zheng, E. Ruggeri, Y. J. Yu, Y. K. Qu, M. Abdi-Jalebi, O. M. Bakr, Z. K. Wang, S. D. Stranks, N. C. Greenham, L. S. Liao, R. H. Friend, *Adv. Mater.* **2021**, *33*, 2103640.
[30] B. Zhao, S. Bai, V. Kim, R. Lamboll, R. Shivanna, F. Auras, J. M. Richter, L. Yang, L. Dai, M. Alsari, X. J. She, L. Liang, J. Zhang, S. Lilliu, P. Gao, H. J. Snaith, J. Wang, N. C. Greenham, R. H. Friend, D. Di, *Nat. Photonics* **2018**, *12*, 783.
[31] S. Wang, Z. Zhang, Z. Tang, C. Su, W. Huang, Y. Li, G. Xing, *Nano Energy* **2021**, *82*, 105712.
[32] K. H. Girish, K. A. Vishnumurthy, T. S. Roopa, *Mater. Today Sustain.* **2022**, *17*, 100090.
[33] D. J. Fairfield, H. Sai, A. Narayanan, J. V. Passarelli, M. Chen, J. Palasz, L. C. Palmer, M. R. Wasielewski, S. I. Stupp, *J. Mater. Chem. A* **2019**, *7*, 1687.
[34] Y. Zhao, P. Zhu, M. Wang, S. Huang, Z. Zhao, S. Tan, T. H. Han, J. W. Lee, T. Huang, R. Wang, J. Xue, D. Meng, Y. Huang, J. Marian, J. Zhu, Y. Yang, *Adv. Mater.* **2020**, *32*, 1907769. .
[35] W. Feng, Y. Zhao, K. Lin, J. Lu, Y. Liang, K. Liu, L. Xie, C. Tian, T. Lyu, Z. Wei, *Adv. Funct. Mater.* **2022**, *32*, 2203371.
[36] H. Li, H. Lin, D. Ouyang, C. Yao, C. Li, J. Sun, Y. Song, Y. Wang, Y. Yan, Y. Wang, Q. Dong, W. C. H. Choy, *Adv. Mater.* **2021**, *33*, 2008820
[37] L. Veeramuthu, F. C. Liang, Z. X. Zhang, C. J. Cho, E. Ercan, C. C. Chueh, W. C. Chen, R. Borsali, C. C. Kuo, *ACS Omega* **2020**, *5*, 8972.
[38] L. Song, L. Huang, Y. Liu, Y. Hu, X. Guo, Y. Chang, C. Geng, S. Xu, Z. Zhang, Y. Zhang, N. Luan, *ACS Appl. Mater. Interfaces* **2021**, *13*, 33199.
[39] D. Wang, Y. Bao, J. Cui, L. Chao, L. Gu, W. Hui, Y. Shen, B. Zhang, Y. Chen, L. Song, *Adv. Funct. Mater.* **2022**, *33*, 2206696. .
[40] R. J. Moon, A. Martini, J. Nairn, J. Simonsen, J. Youngblood, *Chem. Soc. Rev.* **2011**, *40*, 3941.
[41] J. Zeng, R. Li, S. Liu, L. Zhang, *ACS Appl. Mater. Interfaces* **2011**, *3*, 2074.
[42] R. Sabo, A. Yermakov, C. T. Law, R. Elhajjar, *J. Renew. Mater.* **2016**, *4*, 297.
[43] H. Zhu, W. Luo, P. N. Ciesielski, Z. Fang, J. Y. Zhu, G. Henriksson, M. E. Himmel, L. Hu, *Chem. Rev.* **2016**, *116*, 9305.
[44] A. Sultana, M. M. Alam, E. Pavlopoulou, E. Solano, M. Berggren, X. Crispin, D. Zhao, *Chem. Mater.* **2022**, *35*, 1568.
[45] J. Yang, S. Xiong, T. Qu, Y. Zhang, X. He, X. Guo, Q. Zhao, S. Braun, J. Chen, J. Xu, Y. Li, X. Liu, C. Duan, J. Tang, M. Fahlman, Q. Bao, *ACS Appl. Mater. Interfaces* **2019**, *11*, 13491.
[46] H. Y. Chu, J. Y. Hong, C. F. Huang, J. Y. Wu, T. L. Wang, T. M. Wu, R. H. Lee, *Cellulose* **2019**, *26*, 9229.
[47] P. Zhang, N. Gu, L. Song, W. H. Chen, P. Du, X. Yin, J. Xiong, *J. Alloys Compd.* **2021**, *886*, 161247.
[48] X. Li, G. Wu, M. Wang, B. Yu, J. Zhou, B. Wang, X. Zhang, H. Xia, S. Yue, K. Wang, C. Zhang, J. Zhang, H. Zhou, Y. Zhang, *Adv. Energy Mater.* **2020**, *10*, 2001832.
[49] D. W. Kim, C. Hyun, T. J. Shin, U. Jeong, *ACS Nano* **2022**, *16*, 2521.
[50] A. Rubino, L. Caliò, A. García-Bennett, M. E. Calvo, H. Míguez, *Adv. Opt. Mater.* **2020**, *8*, 1901868.
[51] J. Li, H. Jian, Y. Chen, H. Liu, L. Liu, Q. Yao, F. Bi, C. Zhao, X. Tan, J. Jiang, F. Lu, T. Jiu, *Sol. RRL* **2018**, *2*, 1800211.
[52] Y. Zhang, S. Chen, H. Chen, G. Zhang, M. Zhao, C. Zhao, W. Guo, W. Ji, Z. Shi, T. Jiu, *J. Mater. Chem. C* **2020**, *8*, 5894.
[53] T. Wu, Y. Wang, X. Li, Y. Wu, X. Meng, D. Cui, X. Yang, L. Han, *Adv. Energy Mater.* **2019**, *9*, 1803766.
[54] I. C. Smith, E. T. Hoke, D. Solis-Ibarra, M. D. McGehee, H. I. Karunadasa, *Angew. Chem. - Int. Ed.* **2014**, *53*, 11232.
[55] H. Tsai, W. Nie, J. C. Blancon, C. C. Stoumpos, R. Asadpour, B. Harutyunyan, A. J. Neukirch, R. Verduzco, J. J. Crochet, S. Tretiak, L. Pedesseau, J. Even, M. A. Alam, G. Gupta, J. Lou, P. M. Ajayan, M. J. Bedzyk, M. G. Kanatzidis, A. D. Mohite, *Nature* **2016**, *536*, 312.
[56] Y. H. Chang, J. C. Lin, Y. C. Chen, T. R. Kuo, D. Y. Wang, *Nanoscale Res. Lett.* **2018**, *13*, 247.
[57] N. Zhou, B. Huang, M. Sun, Y. Zhang, L. Li, Y. Lun, X. Wang, J. Hong, Q. Chen, H. Zhou, *Adv. Energy Mater.* **2020**, *10*, 1901566.
[58] M. Yuan, L. N. Quan, R. Comin, G. Walters, R. Sabatini, O. Voznyy, S. Hoogland, Y. Zhao, E. M. Beauregard, P. Kanjanaboos, Z. Lu, D. H. Kim, E. H. Sargent, *Nat. Nanotechnol.* **2016**, *11*, 872.
[59] L. Li, S. Tu, G. You, J. Cao, D. Wu, L. Yao, Z. Zhou, W. Shi, W. Wang, H. Zhen, Q. Ling, *Chem. Eng. J.* **2022**, *431*, 133951.
[60] Q. Jiang, Y. Zhao, X. Zhang, X. Yang, Y. Chen, Z. Chu, Q. Ye, X. Li, Z. Yin, J. You, *Nat. Photonics* **2019**, *13*, 460.
[61] K. R. Pradeep, A. Elumalai, R. Viswanatha, *J. Phys. Chem. C* **2022**, *126*, 9813.
[62] M. Ban, Y. Zou, J. P. H. Rivett, Y. Yang, T. H. Thomas, Y. Tan, T. Song, X. Gao, D. Credington, F. Deschler, H. Sirringhaus, B. Sun, *Nat. Commun.* **2018**, *9*, 3892.
[63] V. M. Le Corre, E. A. Duijnstee, O. El Tambouli, J. M. Ball, H. J. Snaith, J. Lim, L. J. A. Koster, *ACS Energy Lett.* **2021**, *6*, 1087.
[64] M. Sajedi Alvar, P. W. M. Blom, G. J. A. H. Wetzelaer, *Nat. Commun.* **2020**, *11*, 4023.
[65] E. A. Duijnstee, J. M. Ball, V. M. Le Corre, L. J. A. Koster, H. J. Snaith, J. Lim, *ACS Energy Lett.* **2020**, *5*, 376.
[66] D. Lu, G. Lv, Z. Xu, Y. Dong, X. Ji, Y. Liu, *J. Am. Chem. Soc.* **2020**, *142*, 11114.
[67] W. Kong, F. Zeng, Z. Su, T. Wang, L. Qiao, T. Ye, L. Zhang, R. Sun, J. Barbaud, F. Li, X. Gao, R. Zheng, X. Yang, *Adv. Energy Mater.* **2022**, *12*, 2202704.
[68] V. S. Chirvony, S. González-Carrero, I. Suárez, R. E. Galian, M. Sessolo, H. J. Bolink, J. P. Martínez-Pastor, J. Pérez-Prieto, *J. Phys. Chem. C* **2017**, *121*, 13381.
[69] H. C. Woo, J. W. Choi, J. Shin, S. H. Chin, M. H. Ann, C. L. Lee, *J. Phys. Chem. Lett.* **2018**, *9*, 4066.
[70] G. Wu, T. Yang, X. Li, N. Ahmad, X. Zhang, S. Yue, J. Zhou, Y. Li, H. Wang, X. Shi, S. (F.) Liu, K. Zhao, H. Zhou, Y. Zhang, *Matter* **2021**, *4*, 582.
[71] Z. M. Gibbs, H. Kim, H. Wang, R. L. White, F. Drymiotis, M. Kaviany, J., G. Snyder, *Appl. Phys. Lett.* **2013**, *103*, 262109.
[72] S. M. Lee, C. J. Moon, H. Lim, Y. Lee, M. Y. Choi, J. Bang, *J. Phys. Chem. C* **2017**, *121*, 26054.
[73] S. Wang, J. Ma, W. Li, J. Wang, H. Wang, H. Shen, J. Li, J. Wang, H. Luo, D. Li, *J. Phys. Chem. Lett.* **2019**, *10*, 2546.
[74] R. Chakraborty, A. Nag, *J. Phys. Chem. C* **2020**, *124*, 16177.
[75] C. Rodà, M. Fasoli, M. L. Zaffalon, F. Cova, V. Pinchetti, J. Shamsi, A. L. Abdelhady, M. Imran, F. Meinardi, L. Manna, A. Vedda, S. Brovelli, *Adv. Funct. Mater.* **2021**, *31*, 2104879.
[76] J. C. Blancon, A. V. Stier, H. Tsai, W. Nie, C. C. Stoumpos, B. Traoré, L. Pedesseau, M. Kepenekian, F. Katsutani, G. T. Noe, J. Kono, S. Tretiak, S. A. Crooker, C. Katan, M. G. Kanatzidis, J. J. Crochet, J. Even, A. D. Mohite, *Nat. Commun.* **2018**, *9*,2254.
[77] J. C. Blancon, H. Tsai, W. Nie, C. C. Stoumpos, L. Pedesseau, C. Katan, M. Kepenekian, C. M. M. Soe, K. Appavoo, M. Y. Sfeir, S. Tretiak, P. M.

Ajayan, M. G. Kanatzidis, J. Even, J. J. Crochet, A. D. Mohite, *Science* **2017**, *355*, 1288.
[78] S. Parveen, K. K. Paul, R. Das, P. K. Giri, *J. Colloid Interface Sci.* **2019**, *539*, 619.
[79] T. D. Siegler, W. A. Dunlap-Shohl, Y. Meng, Y. Yang, W. F. Kau, P. P. Sunkari, C. E. Tsai, Z. J. Armstrong, Y. C. Chen, D. A. C. Beck, M. Meilă, H. W. Hillhouse, *J. Am. Chem. Soc.* **2022**, *144*, 5552.
[80] D. Yang, B. Zhao, T. Yang, R. Lai, D. Lan, R. H. Friend, D. Di, *Adv. Funct. Mater.* **2022**, *32*, 2109495.
[81] Q. Dong, L. Lei, J. Mendes, F. So, *J. Phys. Mater.* **2020**, *3*, 012002.
[82] Y. Wei, Z. Cheng, J. Lin, *Chem. Soc. Rev.* **2019**, *48*, 310.